14

First-Principles Simulation of Magnetic Exchange Force Microscopy on Fe/W(001)

Cesar Lazo, Hendrik Hölscher, Vasile Caciuc, and Stefan Heinze

Abstract. Based on density functional theory, we analyze the contrast mechanisms in magnetic exchange force microscopy (MExFM) and present first-principles calculations of the magnetic exchange force between an iron tip and an Fe monolayer on W(001), which is a model system of a two-dimensional antiferromagnet. Our study reveals that a single Fe atom is not an adequate tip model and we use Fe pyramids of five and 14 atoms. We find that the magnetic exchange forces on the tip atoms in the nearest layer from the apex atom are non-negligible and can be opposite to that on the apex atom. In addition, the apex atom interacts not only with the surface atoms underneath but also with the nearest-neighbors in the surface. We show that structural relaxations of tip and sample due to their interaction depend sensitively on the magnetic alignment of the two systems. As a result, the onset of significant magnetic exchange forces is shifted toward larger tip–sample separations which facilitates their detection in MExFM.

14.1 Introduction

Recent advances in magnetic microscopy techniques [1, 2] allowed spectacular new insights into magnetic properties of nanostructures at surfaces. Among these the spin-polarized scanning tunneling microscope (SP-STM) fascinated many scientists because it is capable to image magnetic structures with atomic resolution [3–9]. However, a scanning tunneling microscope is limited to conducting surfaces and it took many years until the idea presented by Wiesendanger et al. [10] in 1990 was realized: the direct measurement of the magnetic exchange forces between a magnetic tip and a nonconductive magnetic sample. This technique, denoted as magnetic exchange force microscopy (MExFM)[1] is in principle applicable to all magnetic surfaces, i.e., conducting

[1] Please, note that MExFM is different to the often applied *magnetic force microscopy* (MFM) which is well suited to image ferromagnetic domain structures but cannot achieve atomic resolution because data acquisition is based on the detection of long-range magnetostatic forces.

S. Morita et al. (eds.), *Noncontact Atomic Force Microscopy*,
NanoScience and Technology,
DOI: 10.1007/978-3-642-01495-6_14,

as well as insulating systems, which is a valuable advantage compared to the SP-STM technique, e.g., to study molecular magnets. However, the interpretation of measurements by MExFM is not straightforward and the development of theoretical models and tools to understand them is essential.

In the past, first-principles calculations based on density functional theory (DFT) have become indispensable and versatile tools to study nanostructures and to gain an understanding of their electronic, structural, chemical, and magnetic properties. However, within these methods one is frequently limited by the size of the system which can be considered and the level of approximation which is used. To model atomic force microscopy (AFM) experiments, it is essential to calculate the forces between the sample and the tip. For this purpose one has to include, besides the sample, some kind of model tip in the calculations. This fact makes the first-principles simulation of AFM experiments much more challenging than the simulation of STM experiments, in particular, if one allows structural relaxations of tip and sample which can often be crucial. Such realistic theoretical modelling of the interaction between tip and sample has become an integral and essential part of many AFM experiments [11–16]. Nevertheless, there have been only few studies in the past focussing on MExFM [17–22].

The first theoretical study of MExFM was based on a semi-empirical tight-binding calculation by Ness et al. [17] and showed that the magnetic exchange forces between an iron tip and a chromium or a nickel surface should be well below 1 nN. Nonetheless, such forces should be detectable with an atomic force microscope. In this work, however, relaxation of the apex atom and the sample were neglected, and only the *d*-electrons of the system were considered. Later on, Nakamura et al. [18, 19] employed a more sophisticated approach based on DFT to calculate the magnetic exchange force between two Fe(001) surfaces. Forces of a few nN were obtained at a distance of 3 Å. Additionally, it was found that the forces exhibited an oscillatory RKKY-interaction-like behavior as a function of distance. Even above 4 Å, the forces should still be within the experimental resolution limit of AFM. A more recent first-principles study [21, 22] of the magnetic exchange force between a single-iron atom, representing the tip, and the NiO(001) surface has been carried out within the framework of DFT. The calculated MExFM images show a magnetic contrast on the atomic-scale when the single Fe atom tip approaches the surface within 1 Å above the contact point. Therefore, this work predicted the possibility of using MExFM for magnetic imaging with atomic resolution.

These theoretical studies encouraged many experimental attempts to demonstrate MExFM, focussing especially on the (001) surface of the antiferromagnetic insulator NiO [23–28]. However, it took many years before the first successful experiment for NiO(001) was reported [29, 30].

Here, we apply density functional theory using the highly accurate full-potential linearized augmented plane wave (FLAPW) method to study the interaction of a magnetic tip and a magnetic sample which is measured in MExFM but also occurs in SP-STM. We consider one monolayer Fe on W(001) as a model sample system which exhibits a c(2×2) antiferromagnetic structure

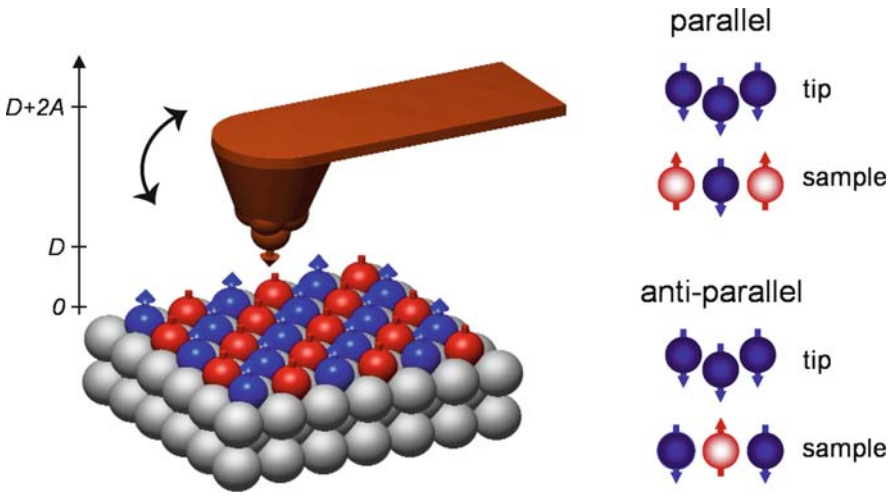

Fig. 14.1. The experimental set-up in magnetic exchange force microscopy. A cantilever with magnetic coating (a few layers of iron for example) oscillates close to the sample surface. The tip–sample forces cause a change of the resonance frequency of the cantilever. Under optimal imaging conditions (UHV, low temperatures, ...) the difference of the forces acting between a parallel or antiparallel configuration of the magnetic moments of the tip-apex and the sample surface atoms may be detected

(Fig. 14.1) and has been resolved by both SP-STM [6] and MExFM [31, 32]. The iron tip is modeled by an Fe pyramid consisting of five atoms and structural relaxations of both tip and sample due to their interaction have been included. Our results show that the relaxations depend sensitively on the magnetic configuration between tip and sample, i.e., whether the tip magnetization is parallel or antiparallel to the moment of the Fe surface atom below. We calculate the magnetic exchange forces, and demonstrate that their measurement in MExFM for this tip–sample system is feasible and even facilitated due to relaxations as their onset is shifted to larger tip–sample separations. We analyze the dependence of the calculated magnetic exchange forces on the tip size and find that a single Fe atom is an inadequate tip model while increasing the tip to 14 atoms changes the forces only quantitatively. By simulating MExFM images, we can explain the contrasts observed in recent experiments [31, 32] and show that they are due to a competition between chemical and magnetic forces.

14.2 Computational Method

To gain insight into the magnetic interactions which occur in an MExFM experiment between an Fe tip and a monolayer of Fe on W(001), we have performed first-principles calculations based on density functional theory within the generalized gradient approximation (GGA) [33] to the exchange-

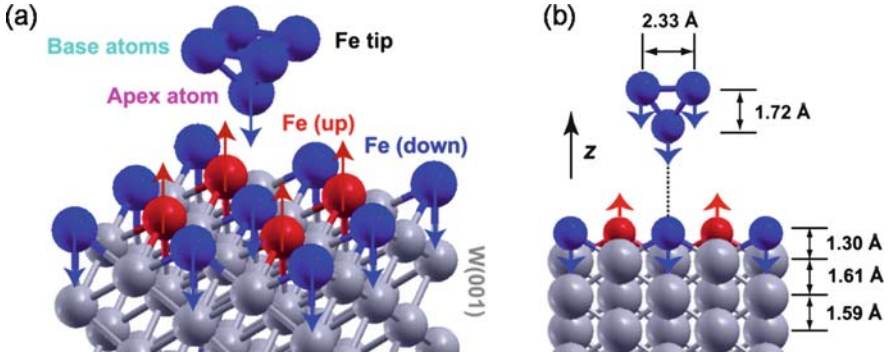

Fig. 14.2. (a) 3D view of the c(4 × 4) unit cell used to calculate the forces between the five Fe atoms pyramid and the Fe monolayer on W(001) which exhibits an antiferromagnetic checkerboard structure. Sites with parallel (p-site) and antiparallel (ap-site) alignment between tip and surface Fe magnetic moments (indicated by *arrows*) are marked. **(b)** Distances given in this side view are obtained after relaxing tip and sample independently. The distance z is defined as tip–sample distance along the approach trajectory (*dotted line*) before considering relaxations due to tip–sample interactions

correlation potential. We apply the full-potential linearized augmented plane wave method as implemented in the WIEN2K [34] code.

We used a ferromagnetic Fe pyramid in bcc-(001) orientation consisting of five Fe atoms as shown in Fig. 14.2. The tip has been fully relaxed, i.e., also the in-plane separation between the base atoms. The coupled system of tip and sample was calculated in a supercell geometry, as shown in Fig. 14.2. The monolayer of Fe on W(001) was modelled by a symmetric slab with five layers of W atoms and one layer of Fe atoms on each side. We used the GGA lattice constant of W (3.181 Å) which is only 0.5% larger than the experimental value (3.165 Å). Tip and surface were initially relaxed independently before considering the coupled system, i.e., the tip–sample interaction.

In two dimensions (2D) our supercell corresponds to a c(4 × 4) unit cell with respect to the Fe/W(001) surface. This choice guarantees that the tip interaction with its lateral image is negligible. The lateral distances between adjacent tips are 9.0 Å for the apex atom and 6.7 Å for the base atoms of the tip. Our supercell is periodic also in z-direction. Choosing a very large vacuum separation of 21 Å between adjacent surfaces, however, allows the tip to approach the surface without interacting with its periodic image. The energy cut-off for the plane wave representation in the interstitial region is $E_{\max}^{\mathrm{wf}} = 11$ Ry and a (3 × 3 × 1) Monkhorst–Pack grid was used for the Brillouin zone integration.

For the relaxed system the separation z is defined as the distance between the center of the tip-apex atom and the probed Fe surface atom before relaxation. It turns out that the relaxation of these atoms is on the order of a few picometers. The force–distance curves discussed in Sect. 14.3 are calculated on two high symmetry points of the surface, which are magnetically different with respect to the magnetization direction of the iron tip pyramid: on-top of an Fe atom with parallel magnetic moment, $F_{\mathrm{p}}(z)$ (p-site), and on top of an Fe atom with antiparallel magnetic moment, $F_{\mathrm{ap}}(z)$ (ap-site). For the simulation of MExFM images, we have calculated an additional force curve on the hollow site, i.e., at the center between the surface atoms.

14.3 Analysis of the Magnetic Exchange Forces

14.3.1 Unrelaxed Tip and Sample

First, we performed separate structural relaxations of tip and sample. Then the tip was approached vertically to the surface of the sample on the p- and ap-site (cf. Fig. 14.2) keeping the internal geometry of the tip and sample fixed, i.e., neglecting structural relaxations due to the tip–sample interaction. The calculated forces acting on the tip are shown in Fig. 14.3a. They display an attractive interaction for the ap- and p-site up to a maximum force of approximately -2.1 and -1.8 nN, respectively, at about 2.7 Å. The difference between the force on the p- and ap-site is the magnetic exchange force (MExF), $F_{\mathrm{ex}}(z)$, defined as

$$F_{\mathrm{ex}}(z) = F_{\mathrm{ap}}(z) - F_{\mathrm{p}}(z) \tag{14.1}$$

which is depicted in Fig. 14.3b by black solid symbols. Interestingly, the magnetic exchange force changes its sign from positive to negative upon

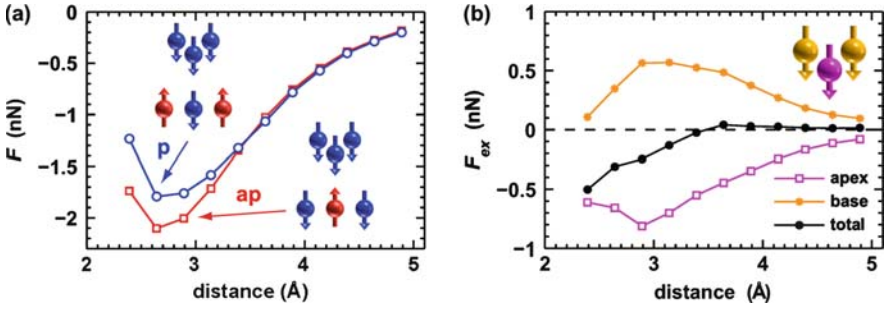

Fig. 14.3. (a) Calculated force–distance curves on the ap-site, $F_{\mathrm{ap}}(z)$, and on the p-site, $F_{\mathrm{p}}(z)$, of the surface (cf. Fig. 14.2), for the tip–sample system neglecting relaxations due to the interaction. **(b)** Total magnetic exchange force and decomposition of the magnetic exchange force into the contributions from different tip atoms

approaching the surface and reaches significant values on the order of 0.2 nN at about 3 Å. The negative sign of the magnetic exchange force indicates a more attractive interaction for an antiparallel alignment of the magnetization of the Fe tip and the Fe surface atom which is being approached (ap-site).

The negative sign of the magnetic exchange force and magnetic exchange energy (see inset of Fig. 14.4b) reveals that antiparallel alignment of tip and sample magnetization, i.e., antiferromagnetic coupling, is favorable. This result may seem rather surprising at first glance as one would intuitively expect ferromagnetic coupling between the interacting Fe atoms of tip and sample. However, the Fe apex atom interacts not only with the Fe surface atom beneath it but also with the four nearest Fe neighbors of this surface atom as will be shown in Sect. 14.3.3. Since the magnetic moments of the Fe atoms on the W(001) surface form an antiferromagnetic checkerboard structure, on the ap-site the magnetization of the tip-apex atom is aligned antiparallel to the moment of the Fe surface atom beneath it and parallel to the moments of the four nearest neighbor Fe surface atoms and vice versa on the p-site. Therefore, if we assume ferromagnetic coupling between individual Fe atoms there is a competition of magnetic exchange interactions with the surface Fe atom and its nearest neighbors.

Further insight into the tip–sample interaction and the forces acting in the system can be obtained by decomposing the total force on the tip (see Fig. 14.3b). The total magnetic exchange force acting on the cluster tip is the sum of the z-components of the magnetic exchange forces acting on the tip-apex atom and the four tip base atoms. As seen in Fig. 14.3b, the magnetic exchange force on the base atoms has an opposite sign to that on the apex atom which leads to a significant reduction of the total magnetic exchange force. As the magnetic exchange force on the apex atom sets in already at much larger tip–sample distances, increasing its contribution to the total magnetic

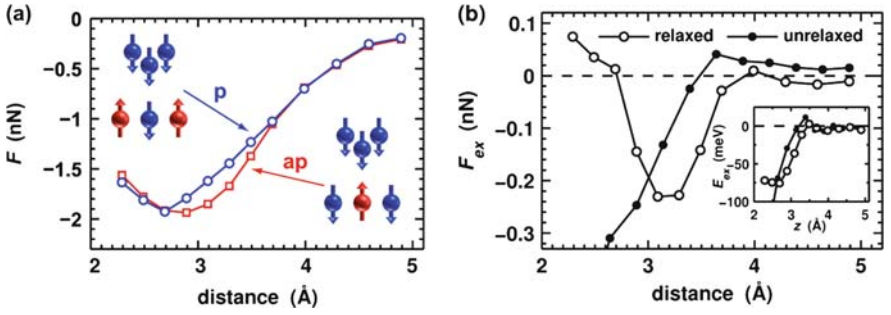

Fig. 14.4. **(a)** Calculated force curves on the ap-site, $F_{\mathrm{ap}}(z)$, and on the p-site, $F_{\mathrm{p}}(z)$, including relaxations of tip and sample due to their interaction. **(b)** Comparison of the magnetic exchange forces between the calculations with and without relaxations as a function of the separation between the unrelaxed tip-apex and probed Fe surface atom. The inset shows the magnetic exchange energies, $E_{\mathrm{ex}}(z) = E_{\mathrm{ap}}(z) - E_{\mathrm{p}}(z)$, for the calculations with and without relaxations

exchange force would greatly enhance the measurable magnetic signal. This result reveals the influence of the interaction of the sample with the tip base atoms. A realistic model of the tip should therefore include not only a single tip-apex atom but at least some tip base atoms. In Sect. 14.3.4, we will explore the influence of the tip size on the obtained magnetic exchange forces in more detail.

14.3.2 Influence of Structural Relaxations

The calculations without structural relaxations presented in Sect. 14.3.1 showed that significant forces act on the tip-apex atom depending on the magnetic configuration between tip and sample. From these results, we conclude that relaxations of tip and sample due to the magnetic interactions should play an important role for the total detectable magnetic exchange force. Therefore, we carried out the same set of calculations as earlier but this time we performed a structural relaxation of the tip-apex atom and the first two layers of the sample at every tip–sample separation.

The force–distance curves shown in Fig. 14.4a explicitly include relaxations due to tip–sample interactions. They look qualitatively similar to the forces for the unrelaxed structure (cf. Fig. 14.3a); however, significant differences arise in the respective magnetic exchange forces which can easily be observed in the splitting between the force curves on the p- and ap-site. On including relaxations, the onset of large magnetic exchange forces shifts towards larger tip–sample distances as seen in Fig. 14.4b. This effect facilitates their experimental detection as the atomic force microscope can be operated at larger distances, i.e., farther from the snap-to-contact point. In addition, $F_{\mathrm{ex}}(z)$ for the relaxed case does not display a marked change of sign at large tip–sample distances. Similar differences are also observed in the magnetic exchange energy for the relaxed and unrelaxed cases (see inset of Fig. 14.4b). Still, antiferromagnetic alignment ($E_{\mathrm{ex}} < 0$) of the Fe tip with respect to the probed Fe surface atom is energetically much more favorable at small separations. As explained in Sect. 14.2, the tip-apex atom interacts not only with the probed Fe surface atom but also with the four neighboring Fe atoms in the surface with antiparallel magnetic moments. Therefore, the negative magnetic exchange energy does not exclude ferromagnetic exchange coupling between the magnetic moments of individual Fe atoms.

These differences in the magnetic exchange forces and energies for the relaxed and unrelaxed case are obviously a result of the relaxation of the tip-apex atom which depends sensitively on its local magnetic configuration with respect to the approached Fe surface atom (see Fig. 14.5a). The tip-apex atom relaxes toward the surface due to the attractive forces and the shape of the relaxation curve. A similar effect is observed for the relaxation of the surface atom being probed which is attracted toward the tip at large distances and repelled at very close separations (see Fig. 14.5b). On the ap-site, the tip-apex atom relaxes about 0.05 Å closer toward the surfaces atom than on the p-site

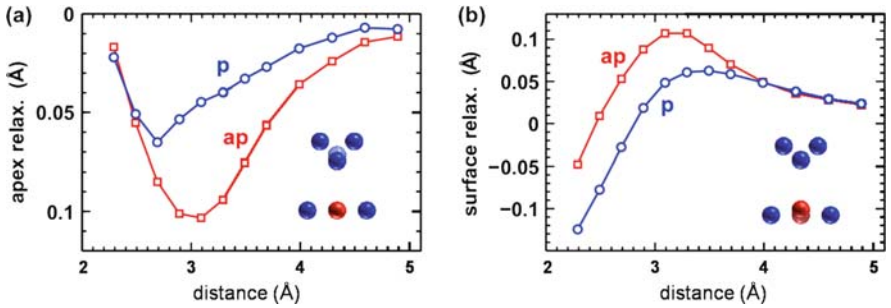

Fig. 14.5. Distance dependence of **(a)** the vertical tip-apex atom relaxation and **(b)** the vertical relaxation of the probed surface Fe atom for the p- and ap-alignment, respectively

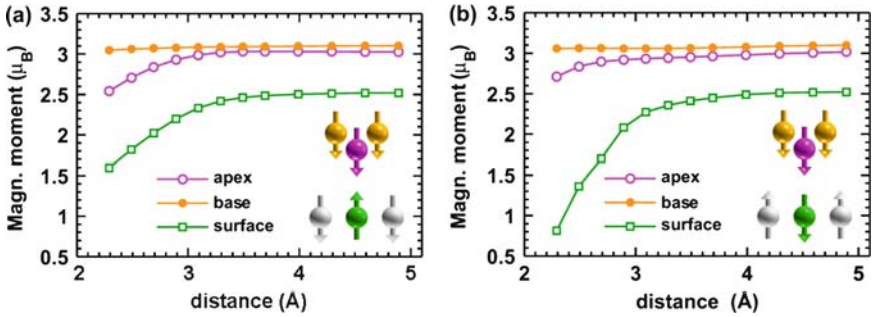

Fig. 14.6. Distance dependence of the absolute magnetic moments of the base (*filled circles*), apex (*circles*), and surface Fe (*squares*) atoms in the case of the five-atoms Fe tip for **(a)** ap-alignment and **(b)** p-alignment between the magnetization of tip and probed Fe surface atom as shown in the insets. These results include structural relaxations of tip and sample

which enhances the magnetic exchange interaction as can be inferred from the force curves of Fig. 14.4.

14.3.3 Electronic and Magnetic Structure Changes due to Tip–Sample Interaction

After analyzing the interaction between tip and sample based on force–distance curves and the resulting relaxations in the earlier sections, we now turn to the modifications of the electronic and magnetic structure due to their interaction. One way to monitor the magnetic interaction is to plot the distance dependence of the magnetic moments of tip-apex atom and surface atom as shown in Fig. 14.6 including structural relaxations.

We find that the magnetic moment of the base atoms remains nearly constant at $m_{\text{base}} \approx 3\,\mu_B$, whereas the moments of the Fe apex and surface atom

decrease as the tip approaches the surface. This decrease becomes significant only at separations below 3 Å, and is due to an increased hybridization between the states of tip apex atom and surface atom. The magnetic moment drop is more pronounced on the p-site than on the ap-site. This result is consistent with the ap-configuration (antiferromagnetic coupling) being energetically more favorable than the p-configuration (inset of Fig. 14.4b), as there is a large energy cost to reduce the magnetic moments from their equilibrium values (obtained at large tip–sample separations).

The origin of the magnetic exchange interaction can be traced to the different electronic interactions in the ap- and p-alignment. In order to study these interactions in detail it is helpful to analyze charge density difference (CDD) plots for the two configurations. This quantity is obtained by subtracting from the charge density of the interacting system consisting of Fe cluster tip and Fe monolayer on W(001) both the charge density of the isolated Fe/W(001) system and that of the isolated Fe cluster tip, using the same atom positions in both cases. The CDD plots visualize the charge transfer associated with the electronic interaction between tip and sample.

Figure 14.7 shows the CDD plots for the ap- and p-alignment at tip–sample distances of $z = 4.9$ and 2.9 Å. At a large separation, there is a small net charge accumulation between the tip-apex atom and the Fe surface atom. Already at this height the interaction depends on the type of spin alignment. The charge accumulation due to tip–sample interaction in the ap-configuration is bound to the Fe surface atom and has a node with the Fe apex atom, while in the p-configuration, it has nodes on both the Fe surface and the tip-apex atom. At a very close distance of $z = 2.9$ Å electronic charge strongly accumulates between the tip-apex atom and the surface Fe atoms, implying a strong electronic interaction between the tip and the surface. The charge accumulation in the ap-alignment is larger than in the p-alignment in agreement with the ap-configuration being energetically more favorable (inset of Fig. 14.4b).

The CDD plots also show that the charge density of the nearest-neighbor Fe atoms (with respect to the probed Fe surface atom) is considerably redistributed on approaching the tip. Therefore, the magnetic exchange coupling of these nearest neighbor Fe atoms with the apex atom of the tip plays an important role to determine whether p- or ap-alignment is more favorable. Similarly, the redistribution of the base atom's charge density indicates a significant contribution to the magnetic exchange interaction between tip and sample.

14.3.4 Influence of Tip Size

One of the more delicate aspects in modeling atomic force microscopy experiments is the geometry used for the tip. Ideally, the tip should consist of thousands of atoms to mimic the tips used in real experiments. However, in practice one is limited by the computational resources required for the calculation. Fortunately, the chemical and magnetic interaction between tip and

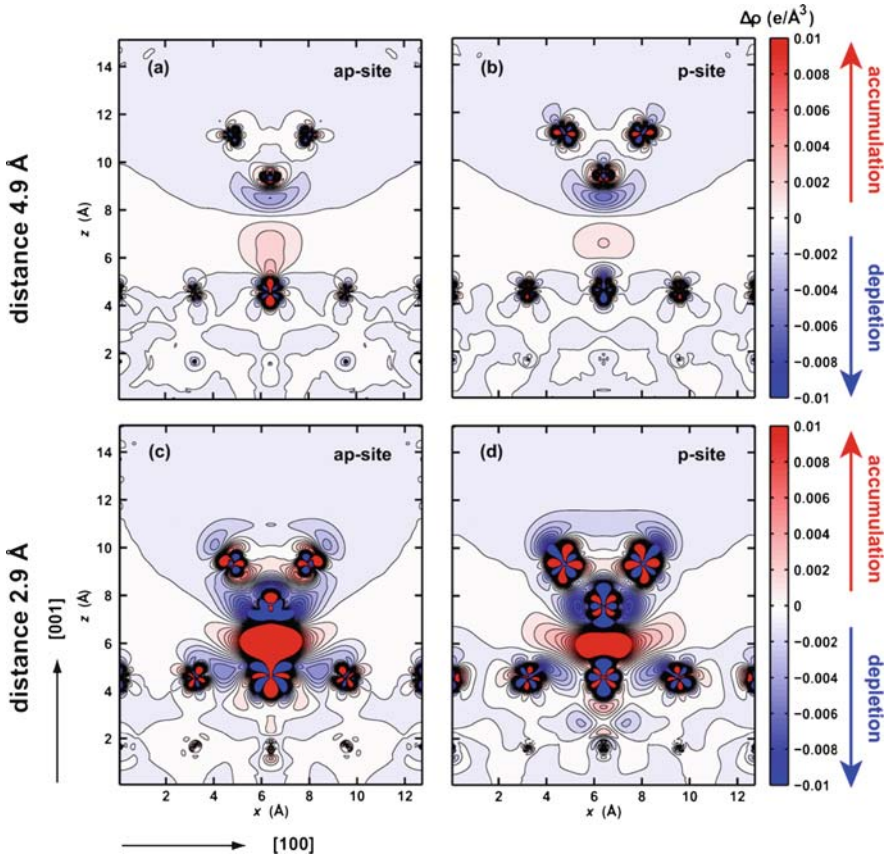

Fig. 14.7. Cross-sectional charge density difference plots along the [011]-direction for the interaction of the five-atoms Fe tip (*top* of each panel) with the Fe monolayer on W(001) (*bottom* of each panel) at tip–sample separations of $z = 4.9$ Å for **(a)** the ap- and **(b)** the p-coupling and at $z = 2.9$ Å for **(c)** the ap- and **(d)** the p-coupling. Zones in *red* and *blue* denote charge accumulation and depletion, respectively. The results presented here correspond to geometries including relaxations due to tip–sample interaction

sample is dominated by the foremost atoms due to the exponential decay of the wave functions while long-range forces can be added based on continuum models [35]. However, the electronic and magnetic properties at the tip-apex are still influenced by the base of the tip used in the model and need to be investigated.

In the past, theoretical calculations have often been carried out using a single Fe atom as an idealized model of the tip to study the magnetic exchange force, e.g., on the NiO(001) surface [20–22]. Here, we assess the validity of such a model using the Fe monolayer on W(001) as a test sample by comparing

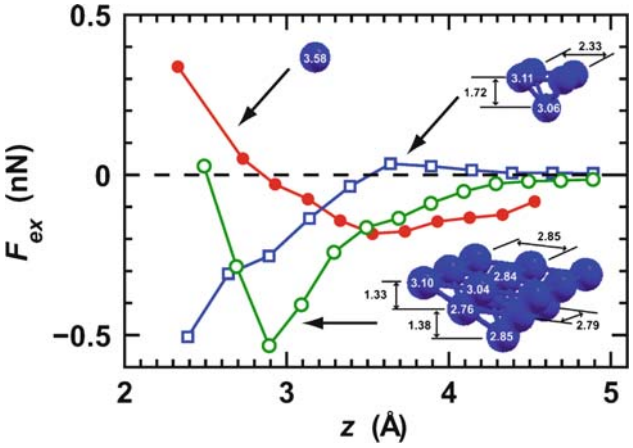

Fig. 14.8. Comparison of the magnetic exchange force $F_{\mathrm{ex}}(z)$ as a function of tip–sample separation z on the Fe monolayer on W(001) using a single Fe atom tip, a five Fe atoms tip, and an Fe tip consisting of 14 atoms. All presented calculations have been performed without structural relaxations of tip and sample due to their interaction. The magnetic moments of the different atoms of the clusters are indicated in *white* in units of the Bohr magneton, μ_B. Additionally, the interlayer distances are indicated in *black* in units of Å (the magnetic moments and geometry values correspond to relaxed geometries of the isolated tip, i.e., without any tip–sample interaction)

calculations using a single Fe atom and the five Fe atoms pyramid tip (discussed in the previous sections) and an even larger 14 Fe atoms tip.

A direct comparison of the magnetic exchange forces for different tip models is given in Fig. 14.8. Obviously, the magnetic exchange force obtained for a single Fe atom tip is even qualitatively different from both pyramid-type tips. At large separations, the magnetic exchange forces are much larger than for the pyramid tips, while they have the opposite sign at close distance. From these calculations, it is quite clear that a single Fe atom cannot mimic the magnetic exchange forces between a magnetic tip and sample. If we compare the two pyramid-type Fe tips, on the other hand, the general shape of the curve is very similar and the smaller tip gives qualitatively the same result. However, the magnetic exchange forces for the bigger Fe tip are significantly enhanced and set in at much larger tip–sample distances which is of crucial importance in experiments.

14.4 Simulation of MExFM Images

Since it is not possible to compare directly the earlier calculated tip–sample forces with the available experimental images [32], a simulation of MExFM images is required. For this procedure, it is essential to consider the long-range

tip–sample interaction caused by the van der Waals forces acting between the macroscopic tip and the sample. As in other studies (see, e.g., [16]), we model the macroscopic part of the tip by a sphere with radius R. The corresponding long-range force is given by $F_{\mathrm{vdW}}(z) = -(A_{\mathrm{H}}R)/(6z^2)$, where A_{H} is the Hamaker constant. For symmetry reasons, we have obtained the total tip–sample force as sum of the long- and short-range forces at three distinct lattice sites: the p-site, ap-site, and the hollow site (h-site). The experimentally measured frequency shift Δf can then be calculated from the numerical solution of the integral [36]

$$\Delta f(D) = \frac{1}{\sqrt{2}\pi}\frac{f_0}{c_z A^{3/2}}\int_D^{\infty}\frac{F_{\mathrm{ts}}(z)}{\sqrt{z-D}}\mathrm{d}z. \tag{14.2}$$

For simplicity we use here reduced units, i.e., the normalized frequency shift $\gamma = c_z A^{3/2}\Delta f/f_0$. This quantity is independent of the actual experimental parameters A, c_z and f_0 [35] and is plotted in Fig. 14.9(a). To simulate constant γ images, we choose a suitable value γ_{c} and determine the corresponding nearest tip–sample distance at the lower turnaround point of the cantilever oscillation, D, numerically by solving $\gamma(D) = \gamma_{\mathrm{c}}$. As a result, we obtain the corrugation amplitudes at the three distinctive lattice sites as a function of γ, and hence, D (see the arrows in Fig. 14.9a). Based on these curves we have simulated complete MExFM images, Fig. 14.9b–d, using the first two non-constant terms of a two-dimensional Fourier expansion [16, 37].

The analysis reveals that the magnetic contrast depends sensitively on the actual normalized frequency shift, i.e., the nearest tip–sample distance D.

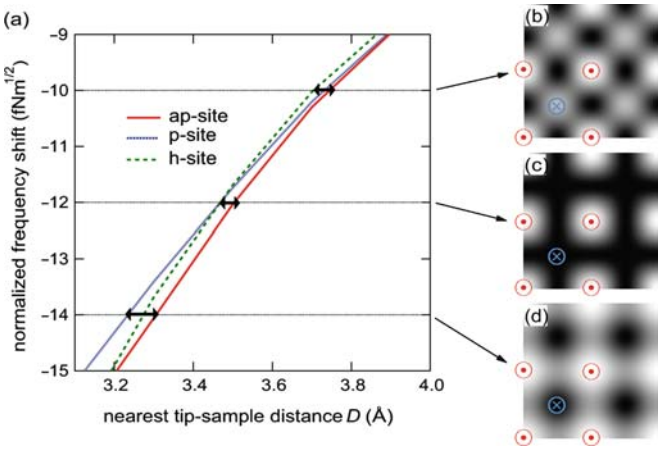

Fig. 14.9. (**a**) Calculated height difference between p-, ap- and h-site, respectively, depending on γ_{c} and hence D. Long-range van der Waals forces were added assuming $R = 8\,\mathrm{nm}$ and $A_{\mathrm{H}} = 0.1\,\mathrm{aJ}$. The p-site defines the zero line. (**b–d**) Simulated MExFM images at γ_{c} of -14, -12, and $-10\,\mathrm{fNm}^{1/2}$ corresponding to $D = 3.2, 3.5$, and $3.7\,\mathrm{Å}$, respectively

At large D, Fig. 14.9d, the chemical contrast dominates and the ap- and p-site appear as local maxima of only slightly different height due to a small magnetic exchange force of about 0.06 nN. At very small D, Fig. 14.9b, the magnetic forces dominate and Fe atoms with opposite magnetic moments appear as minima and maxima. At intermediate D, p- and h-site exhibit nearly the same height level and become indistinguishable. At the crossing point in Fig. 14.9a, they are exactly equal and only the ap-sites appear as maxima, (cf. Fig. 14.9c). Note that chemical and magnetic forces are both present and are of considerable magnitude, but the total forces at p- and h-site are equal. The contrast in Fig. 14.9c fits best to the experimental image presented in Chap. 13 of this book [32]. In a different experiment Schmidt et al. [31] also observed a contrast pattern similar to Fig. 14.9d, which is expected to appear at relatively large separations with smaller magnetic contrast. However, up to now, experimental data never exhibited a contrast pattern as shown in the simulated image Fig. 14.9b, probably because stable imaging is difficult at such close distances.

14.5 Summary

Utilizing density functional theory we have analyzed the magnetic exchange forces present in MExFM of an Fe monolayer on W(001), a two-dimensional itinerant antiferromagnet, using an Fe tip. Our study revealed that a single Fe atom is not an adequate tip model as the obtained magnetic exchange forces are even qualitatively different from those calculated with pyramid tips of five and 14 atoms. Surprisingly, the magnetic exchange forces on the tip atoms in the nearest layer from the apex atom are non-negligible and can be opposite to that on the apex atom. We demonstrate that the apex atom interacts not only with the surface atom directly underneath but also with nearest-neighbor atoms in the surface. Interestingly, structural relaxations of tip and sample due to their interaction depend sensitively on the magnetic alignment of the two systems. As a result the onset of significant magnetic exchange forces is shifted toward larger tip–sample separations which facilitates their detection in MExFM. Based on the first-principles calculation of the tip–sample forces we simulated MExFM images of the Fe monolayer on W(001) which showed contrast patterns in excellent agreement with available experimental data [32].

The computations shown here were performed at the Hamburg University of Technology, the Norddeutscher Verbund für Hoch- und Höchstleistungsrechnen (HLRN), and the Forschungszentrum Jülich (JUMP). We acknowledge financial support from the DFG (Grants No. HO 2237/3-1 and HE 3292/4-1). S.H. thanks the Stifterverband für die Deutsche Wissenschaft and the Interdisciplinary Nanoscience Center Hamburg for financial support.

References

1. I.S. Osborne, Science **294**, 1483 (2001)
2. M.R. Freeman, B.C. Choi, Science **294**, 1484 (2001)
3. S. Heinze, M. Bode, A. Kubetzka, O. Pietzsch, X. Nie, S. Blügel, R. Wiesendanger, Science **288**, 1805 (2000)
4. D. Wortmann, S. Heinze, P. Kurz, G. Bihlmayer, S. Blügel, Phys. Rev. Lett. **86**(18), 4132 (2001)
5. H. Yang, A.R.Smith, M. Prikhodko, W.R.L. Lambrecht, Phys. Rev. Lett. **89**, 226101 (2002)
6. A. Kubetzka, P. Ferriani, M. Bode, S. Heinze, G. Bihlmayer, K. von Bergmann, O. Pietzsch, S. Blügel, R. Wiesendanger, Phys. Rev. Lett. **94**, 087204 (2005)
7. M. Bode, Rep. Prog. Phys. **66**, 523 (2003)
8. C.L. Gao, U. Schlickum, W. Wulfhekel, J. Kirschner, Phys. Rev. Lett. **98**, 107203 (2007)
9. C.L. Gao, A. Ernst, A. Winkelmann, J. Henk, W. Wulfhekel, P. Bruno, J. Kirschner, Phys. Rev. Lett. **100**, 237203 (2008)
10. R. Wiesendanger, D. Bürgler, G. Tarrach, A. Wadas, D. Brodbeck, G.G. Güntherodt, H.-J. Güntherodt, R.J. Gambino, R. Ruf, J. Vac. Sci. Technol. B **9**, 519 (1990)
11. R. Pérez, M.C. Payne, I. Stich, K. Terakura, Phys. Rev. Lett. **78**, 678 (1997)
12. R. Pérez, I. Štich, M.C. Payne, K. Terakura, Phys. Rev. B **58**, 10835 (1998)
13. V. Caciuc, H. Hölscher, S. Blügel, H. Fuchs, Phys. Rev. Lett. **96**, 016101 (2006)
14. Y. Sugimoto, P. Pou, M. Abe, P. Jelinek, R. Perez, S. Morita, O. Custance, Nature **446**, 64 (2007)
15. N. Atodiresei, V. Caciuc, S. Blügel, H. Hölscher, Phys. Rev. B **77**, 153408 (2008)
16. V. Caciuc, H. Hölscher, D. Weiner, H. Fuchs, A. Schirmeisen, Phys. Rev. B. **77**, 045411 (2008)
17. H. Ness, F. Gautier, Phys. Rev. B **52**, 7352 (1995)
18. K. Nakamura, H. Hasegawa, T. Oguchi, K. Sueoka, K. Hayakawa, K. Mukasa, Phys. Rev. B **56**, 3218 (1997)
19. K. Nakamura, T. Oguchi, H. Hasegawa, K. Sueoka, K. Hayakawa, K. Mukasa, Appl. Surf. Sci. **142**, 433 (1999)
20. A.S. Foster, A.L. Shluger, Surf. Sci. **490**, 211 (2001)
21. H. Momida, T. Oguchi, J. Phys. Soc. Jpn. **72**, 588 (2003)
22. H. Momida, T. Oguchi, Surf. Sci. **590**, 42 (2005)
23. H. Hosoi, K. Sueoka, K. Hayakawa, K. Mukasa, Appl. Surf. Sci. **157**, 218 (2000)
24. H. Hosoi, K. Sueoka, K. Mukasa, Nanotechnology **15**, 505 (2004)
25. H. Hölscher, S.M. Langkat, A. Schwarz, R. Wiesendanger, Appl. Phys. Lett. **81**, 4428 (2002)
26. S.M. Langkat, H. Hölscher, A. Schwarz, R. Wiesendanger, Surf. Sci. **527**, 12 (2003)
27. R. Hoffmann, M.A. Lantz, H.J. Hug, P.J.A. van Schendel, P. Kappenberger, S. Martin, A. Baratoff, H.J. Güntherodt, Phys. Rev. B **67**, 085402 (2003)
28. M. Schmid, J. Mannhart, F.J. Giessibl, Phys. Rev. B **77**, 045402 (2008)
29. U. Kaiser, A. Schwarz, R. Wiesendanger, Nature **446**, 522 (2007)
30. U. Kaiser, A. Schwarz, R. Wiesendanger, Phys. Rev. B **77**, 153408 (2008)
31. R. Schmidt, C. Lazo, H. Hölscher, U.H. Pi, V. Caciuc, A. Schwarz, R. Wiesendanger, S. Heinze, Nano Lett. **9**, 200 (2009)

32. A. Schwarz, U. Kaiser, R. Schmidt, R. Wiesendanger, in *Magnetic Exchange Force Microscopy: Experiment*, eds. by S. Morita, F.-J. Giessibl, R. Wiesendanger. NC-AFM, vol II (Springer-Verlag Berlin-Heidelberg, 2009)
33. J.P. Perdew, K. Burke, M. Ernzerhof, Phys. Rev. Lett. **77**(18), 3865 (1996)
34. G.K.H. Madsen, P. Blaha, K. Schwarz, E. Sjöstedt, L. Nordström, Phys. Rev. B **64**(19), 195134 (2001)
35. F.J. Giessibl, Phys. Rev. B **1997**, 16010 (1997)
36. U. Dürig, Appl. Phys. Lett. **75**, 433 (1999)
37. N. Sasaki, H. Aizawa, M. Tsukada, Appl. Surf. Sci. **157**, 367 (2000)